

Trajectories in phase diagrams, growth processes and computational complexity: how search algorithms solve the 3-Satisfiability problem.

Simona Cocco ^{*} and Rémi Monasson [†]

CNRS-Laboratoire de Physique Théorique de l'ENS, 24 rue Lhomond, 75005 Paris, France

Most decision and optimization problems encountered in practice fall into one of two categories with respect to any particular solving method or algorithm: either the problem is solved quickly (easy) or else demands an impractically long computational effort (hard). Recent investigations on model classes of problems have shown that some global parameters, such as the ratio between the constraints to be satisfied and the adjustable variables, are good predictors of problem hardness and, moreover, have an effect analogous to thermodynamical parameters, e.g. temperature, in predicting phases in condensed matter physics [Monasson et al., Nature 400 (1999) 133-137]. Here we show that changes in the values of such parameters can be tracked during a run of the algorithm defining a trajectory through the parameter space. Focusing on 3-Satisfiability, a recognized representative of hard problems, we analyze trajectories generated by search algorithms using growth processes statistical physics. These trajectories can cross well defined phases, corresponding to domains of easy or hard instances, and allow to successfully predict the times of resolution.

PACS Numbers : 05.10, 05.70, 89.80

Consider a set of N Boolean variables (that can be either true or false) and a set of $M = \alpha N$ constraints (called clauses), each of which being the logical OR of three variables or of their negations, see Figure 1. Then, try to figure out whether there exists or not an assignment of variables satisfying all clauses (called solution).

This problem, called 3-Satisfiability (3-SAT), is among the most difficult ones to solve as its size N becomes large. It is a fundamental conjecture of computer science that no method exists to solve 3-SAT efficiently [1], *i.e.* in time growing at most polynomially with N . In practice, one therefore resorts to methods that need, *a priori*, exponentially large computational resources. One of these algorithms, the ubiquitous Davis–Putnam–Loveland–Logemann (DPLL) solving procedure [6,2,4], is illustrated in Figure 1. DPLL operates by trials and errors, the sequence of which can be graphically represented as a search tree made of nodes connected through edges, see Figure 1. Examples of search trees for satisfiable (sat) or unsatisfiable (unsat) instances are shown Figure 2. Computational complexity is the amount of operations performed by the solving algorithm; we follow the convention that it is measured by the size of the search tree, *i.e.* the number of nodes.

Complexity may, in practice, vary enormously with the instance, that is, the set of clauses, under consideration. To understand why instances are easy or hard to solve, computer scientists have focused on model classes of 3-SAT instances. Probabilistic models, that define distributions of random instances controlled by few parameters, are particularly useful to shed light on the onset of complexity. An example, that has attracted a lot of attention over the past years, is random 3-SAT: all clauses are drawn randomly and each variable negated or left unchanged with equal probabilities. Experiments [2,3] and theory [10] indicate that clauses can almost surely always (respectively never) be simultaneously satisfied if α is smaller (resp. larger) than a critical threshold $\alpha_C \simeq 4.3$ as soon as M, N go to infinity at fixed ratio α . This phase transition [5,10] is accompanied by a drastic peak of hardness at threshold [2,3], see Figure 3. A complete understanding of this pattern of complexity has been lacking so far.

In this letter we argue that search algorithms induce a dynamical evolution of the computational problem to be solved. We shall show how this complex and non-Markovian dynamics can be closely related to (surface) growth processes. Statistical mechanics concepts and tools thus allow to predict analytically and understand computational complexity. For the sake of clarity, we shall report technical details in another and extended paper [15].

As shown in Figure 1, the action of DPLL on an instance of 3-SAT causes the reduction of 3-clauses to 2-clauses. We use a mixed 2+p-SAT distribution [5], where p is the fraction of 3-clauses, to model what remains of the input instance at a node of the search tree. Using experiments and methods from statistical mechanics [10], the threshold line $\alpha_C(p)$ may be obtained with the results shown in Figure 4 (full line). The phase diagram of 2+p-SAT is the natural space in which the DPLL dynamic takes place. An input 3-SAT instance with ratio α shows up on the right

^{*}Current address: Department of Physics, The University of Illinois at Chicago, 845 W. Taylor St., Chicago IL 60607.

[†]Current address: The James Franck Institute, The University of Chicago, 5640 S. Ellis Av., Chicago IL 60637.

vertical boundary of Figure 4 as a point of coordinates ($p = 1, \alpha$). Under the action of DPLL, the representative point moves aside from the 3-SAT axis and follows a trajectory. The location of this trajectory in the phase diagram allows a precise understanding of the search tree structure and of complexity. (in the following, we consider the trajectories generated by DPLL using the GUC heuristics [9] – see caption of Figure 1 – but our calculation could be repeated for other rules [2,3,9,12]).

At sufficiently small ratios $\alpha < \alpha_L \simeq 3.003$, DPLL easily finds a solution [9,12]. The search tree has a unique branch (sequence of edges joining the top node to the extremity). This branch grows as the fraction t of variables assigned by DPLL increases and terminates with a solution, see Figure 2A. Each node along the branch carries a 2+p-SAT instance with characteristic parameters p and α . The knowledge of the latter as functions of the “depth” t of the node, first established by Chao and Franco [9], allows us to draw the trajectory followed by the instance under the action of DPLL in Figure 4. The trajectory, indicated by a light dashed line, first heads to the left and then reverses to the right until reaching a point on the 3-SAT axis at small ratio without ever leaving the sat region. Further action of DPLL leads to a rapid elimination of the remaining clauses and the trajectory ends up at the right lower corner S, where a solution is achieved. Thus, in the range of ratios $\alpha < \alpha_L \simeq 3.003$, 3-SAT is easy to solve: the computational complexity scales linearly with the size N , see Figure 3.

For ratios above threshold ($\alpha > \alpha_C \simeq 4.3$), instances have (almost) never a solution but a considerable amount of backtracking is necessary before proving that clauses are incompatible. As shown in Figure 2B, a generic unsat tree includes many branches. The number B of branches is related to the number Q of nodes through the relation $Q = B - 1$ valid for any complete tree, check Figure 2B. Complexity grows exponentially [13] as $2^{N\omega}$. We have experimentally counted directly Q or, alternatively, B , and averaged the corresponding logarithms ω over a large number of instances. Results have then been extrapolated to the $N \rightarrow \infty$ limit [15] and are reported in Table 1.

We have analytically computed ω as a function of α , extending to the unsat region the probabilistic analysis of DPLL. The search tree of Figure 2B is the output of a sequential process: nodes and edges are added by DPLL through successive descents and backtrackings. We have imagined a different building up, that results in the same complete tree but can be mathematically analysed: the tree grows in parallel, layer after layer. A new layer is added by assigning, according to DPLL heuristic, one more variable along each living branch. As a result, some branches split, others keep growing and the remaining ones carry contradictions and die out. At a given depth (fraction of assigned variables) t in the tree, each branch carries a 2+p-SAT instance, with characteristic parameters p, α . Its further evolution can be well approximated by a Markovian stochastic process that depends only on p and α . This approximation permits to write an evolution equation for the logarithm $\omega(p, \alpha; t)$ of the average number of branches with parameters p, α as the depth t increases,

$$\frac{\partial \omega}{\partial t} = \mathcal{H} \left[p, \alpha, \frac{\partial \omega}{\partial p}, \frac{\partial \omega}{\partial \alpha}, t \right] \quad , \quad (1)$$

\mathcal{H} incorporates the details of the splitting heuristics [14]. Partial differential equation (1) is analogous to growth processes encountered in statistical physics [8]. The surface ω , growing with “time” t above the bidimensional plane p, α , describes the whole branches distribution. Exponentially dominant branches are given by the top of the distribution; the coordinates $p(t), \alpha(t)$ of the maximum of ω define the tree trajectories on Figure 4. The hyperbolic line indicates the halt points, where contradictions prevent tree trajectories from further growing. Along the trajectory, ω grows from 0, on the right vertical axis up to some final positive value on the halt line. This value is our theoretical prediction for the logarithm of the complexity (divided by N). Values of ω , obtained for $4.3 < \alpha < 20$ by solving equation (1) compare very well with numerical results, see Table 1.

The intermediate region $\alpha_L < \alpha < \alpha_C$ juxtaposes the two previous behaviours, see tree Figure 2C. The branch trajectory, started from the point ($p = 1, \alpha$) corresponding to the initial 3-SAT instance, hits the critical line $\alpha_c(p)$ at some point G with coordinates (p_G, α_G) . The algorithm then enters the unsat phase and generates 2+p-SAT instances with no solution. A dense subtree, that DPLL has to go through entirely, forms below G till the halt line, see tree trajectory in Figure 4. From our theoretical framework, the logarithm ω of the size of this subtree can be analytically predicted. G is the highest backtracking node in the tree (see Figure 2C) reached back by DPLL, since nodes above G are located in the sat phase and carry 2+p-SAT instances with solutions. We have checked experimentally this scenario for $\alpha = 3.5$. The coordinates of the average highest backtracking node, $(p_G \simeq 0.78, \alpha_G \simeq 3.0)$, coincide with the analytically computed intersection of the single branch trajectory and the critical line $\alpha_c(p)$, see Figure 4. As for complexity, experiments on 3-SAT instances at $\alpha = 3.5$ or on 2+0.78-SAT instances at $\alpha_G = 3.0$ are in good agreement with theoretical calculations of ω , see Table 1. As a conclusion, the structure of search trees for 3-SAT reflects the existence of a critical line for 2+p-SAT instances. The latter may be found back as the locus of highest backtracking nodes reached from all initial 3-SAT ratios α in the intermediate range.

In conclusion, we have shown that statistical physics tools can be useful to study the solving complexity of branch and bound algorithms [1,4] applied to hard combinatorial optimization or decision problems. The phase diagram of Figure 4 affords a qualitative understanding of the probabilistic complexity of DPLL variants on random instances. This view may reveal the nature of the complexity of search algorithms for SAT and related NP-complete problems [1]. In the sat phase, branch trajectories are related to polynomial time computations while in the unsat region, tree trajectories lead to exponential calculations. Depending on the starting point (ratio α of the 3-SAT instance), one or a mixture of these behaviours is observed. Figure 4 furthermore gives some insights to improve the search algorithm. In the unsat region, trajectories must be as horizontal as possible (to minimize their length) but resolution is necessarily exponential [13]. In the sat domain, heuristics making trajectories steeper could avoid the critical line $\alpha_C(p)$ and solve 3-SAT polynomially up to threshold.

Acknowledgements: We are grateful to J. Franco for his encouragements and numerous suggestions in the writing of this work. We also thank A. Hartmann and M. Weigt for their interest in our results.

- [1] Garey, M. & Johnson, D.S. *Computers and Intractability; A guide to the theory of NP-completeness* (W.H. Freeman and Co., San Francisco, 1979).
- [2] Crawford, J. & Auton, L. *Proc. 11th Natl. Conference on Artificial Intelligence (AAAI-93)*, 21–27 (The AAAI Press / MIT Press, Cambridge, MA, 1993).
- [3] Hogg, T., Huberman, B.A. & Williams, C. (eds.) *Frontiers in problem solving: phase transitions and complexity. Artificial Intelligence* **81**(I & II) (1996).
- [4] Hayes, B. *American Scientist* **85**(2), 108–112 (1996).
- [5] Monasson, R., Zecchina, R., Kirkpatrick, S., Selman, B. & Troyansky, L. *Nature* **400**, 133–137 (1999).
- [6] Davis, M. & Putnam, H. *J. Assoc. Comput. Mach.* **7**, 201–215 (1960).
- [7] Mézard, M., Parisi, G. & Virasoro, M.A. *Spin Glass Theory and Beyond* (World Scientific, Singapore, 1987) and references therein.
- [8] McKane, A., Droz, M., Vannimenus, J. & Wolf, D. (eds.) *Scale invariance, interfaces, and non-equilibrium dynamics*. (Nato Asi Series B: Physics vol. 344, Plenum Press, New-York, 1995).
- [9] Chao, M.T. & Franco, J. *Information Science* **51**, 289–314 (1990).
- [10] Monasson, R. & Zecchina, R. *Phys. Rev. E* **56**, 1357–1370 (1997).
- [11] Beame, P., Karp, R., Pitassi, T. & Saks, M. *ACM Symp. on Theory of Computing (STOC98)*, 561–571 (Assoc. Comput. Mach., New York, 1998).
- [12] Frieze, A. & Suen, S. *Journal of Algorithms* **20**, 312–335 (1996).
- [13] Chvátal, V. & Szemerédi, E. *Journal of the ACM* **35**, 759–768 (1988).
- [14] In terms of the densities of 2- and 3-clauses, $c_2 = \alpha(1-t)(1-p)$, $c_3 = \alpha(1-t)p$, and of the partial derivatives $z_2 = \partial\omega/\partial c_2$, $z_3 = \partial\omega/\partial c_3$, we have for the GUC heuristics $\mathcal{H}(c_2, c_3, z_2, z_3; t) = \log_2 \nu(z_2) + [3 c_3 (e^{z_3}(1 + e^{-z_2})/2 - 1) + c_2 (\nu(z_2) - 2)]/(1-t)/\log 2$ where $\nu(z_2) = e^{z_2} (1 + \sqrt{4e^{-z_2} + 1})/2$. We have solved eqn. (1) by expanding \mathcal{H} at the linear order in z_2, z_3 . Notice that theory concentrates on the logarithm of the average number of branches. This annealed approximation of ω is very accurate above threshold [15].
- [15] S. Cocco, R. Monasson, in preparation.

TABLE

Ratio α clause/var.	Experiments		Theory
	nodes	branches	
20	0.0153 ± 0.0002	0.0151 ± 0.0001	0.0152
15	0.0207 ± 0.0002	0.0206 ± 0.0001	0.0206
10	0.0320 ± 0.0005	0.0317 ± 0.0002	0.0319
7	0.0482 ± 0.0005	0.0477 ± 0.0005	0.0477
4.3	0.089 ± 0.001	0.0895 ± 0.001	0.0875
3.5	0.045 ± 0.005	0.044 ± 0.005	
3.0 ($p = 0.78$)	0.042 ± 0.002	0.041 ± 0.003	0.0453

Table 1: Logarithm of the complexity ω from measures of search tree sizes (nodes and branches) and theory [14]. Experimental results obtained for $\alpha = 3.5$ (sat phase) are compared to the complexity of the unsat tree built from hit point G ($p_G = 0.78, \alpha_G = 3$), see Figure 4. Uncertainties on ω are larger due to finite size critical fluctuations on the location of G . For $\alpha \gg 1$, our theoretical prediction $\omega = (3 + \sqrt{5})[\ln((1 + \sqrt{5})/2)]^2/(6 \ln 2)/\alpha \simeq 0.292/\alpha$ seems to be exact [11]; indeed, the search tree becomes small enough to justify the decorrelation of branches done in (1).

FIGURE CAPTIONS

Figure 1: Example of 3-SAT instance and Davis–Putnam–Loveland–Logemann resolution. **Step 0.** The instance consists of $M = 5$ clauses involving $N = 4$ variables that can be assigned to true (T) or false (F). \bar{w} means (NOT w) and v denotes the logical OR. The search tree is empty. **1.** DPLL randomly selects a variable among the shortest clauses and assigns it to satisfy the clause it belongs to, e.g. $w = T$ (splitting with the Generalized Unit Clause –GUC– heuristic) [6,9]. A node and an edge symbolising respectively the variable chosen (w) and its value (T) are added to the tree. **2.** The logical implications of the last choice are extracted: clauses containing w are satisfied and eliminated, clauses including \bar{w} are simplified and the remaining ones are left unchanged. If no unitary clause (*i.e.* with a single variable) is present, a new choice of variable has to be made. **3.** Splitting takes over. Another node and another edge are added to the tree. **4.** Same as step 2 but now unitary clauses are present. The variables they contain have to be fixed accordingly. **5.** The propagation of the unitary clauses results in a contradiction. The current branch dies out and gets marked with C. **6.** DPLL backtracks to the last split variable (x), inverts it (F) and creates a new edge. **7.** Same as step 4. **8.** The propagation of the unitary clauses eliminates all the clauses. A solution S is found and the instance is satisfiable. For an unsatisfiable instance, unsatisfiability is proven when backtracking (see step 6) is not possible anymore since all split variables have already been inverted. In this case, all the nodes in the final search tree have two descendent edges and all branches terminate by a contradiction C.

Figure 2: Types of search trees generated by the DPLL solving procedure. **A.** *simple branch*: the algorithm finds easily a solution without ever backtracking. **B.** *dense tree*: in the absence of solution, the algorithm builds a “bushy” tree, with many branches of various lengths, before stopping. **C.** *mixed case, branch + tree*: if many contradictions arise before reaching a solution, the resulting search tree can be decomposed in a single branch followed by a dense tree. The junction G is the highest backtracking node reached back by DPLL.

Figure 3: Complexity of 3-SAT solving for three problem sizes and averaged over 10,000 randomly drawn samples.

Figure 4: Phase diagram of 2+p-SAT and dynamical trajectories of DPLL. The threshold line $\alpha_C(p)$ (bold full line) separates sat (lower part of the plane) from unsat (upper part) phases. Extremities lie on the vertical 2-SAT (left) and 3-SAT (right) axis at coordinates $(p = 0, \alpha_C = 1)$ and $(p = 1, \alpha_C \simeq 4.3)$ respectively. Departure points for DPLL trajectories are located on the 3-SAT vertical axis and the corresponding values of α are explicitly given. Dashed curves represent tree trajectories in the unsat region (thick lines, black arrows) and branch trajectories [9] in the sat phase (thin lines, empty arrows). Arrows indicate the direction of “motion” along trajectories parametrised by the fraction t of variables set by DPLL. For small ratios $\alpha < \alpha_L$, branch trajectories remain confined in the sat phase and end in S of coordinates $(1, 0)$, where a solution is found. At $\alpha_L \simeq 3.003$, the single branch trajectory hits tangentially the threshold line in T of coordinates $(2/5, 5/3)$. In the intermediate range $\alpha_L < \alpha < \alpha_C$, the branch trajectory intersects the threshold line at some point G (that depends on α). A dense tree then grows in the unsat phase, as happens when 3-SAT departure ratios are above threshold $\alpha > \alpha_C \simeq 4.3$. The tree trajectory halts on the dot-dashed curve $\alpha \simeq 1.259/(1 - p)$ where the tree growth process stops, see text. At this point, DPLL has reached back the highest backtracking node in the search tree, that is, the first node when $\alpha > \alpha_C$, or node G for $\alpha_L < \alpha < \alpha_C$. In the latter case, a solution can be reached from a new descending branch while, in the former case, unsatisfiability is proven.

step	clauses	search tree
0	$w \vee \bar{x} \vee y$ $\bar{w} \vee x \vee z$ $\bar{w} \vee \bar{x} \vee \bar{y}$ $\bar{w} \vee \bar{x} \vee y$ $x \vee y \vee \bar{z}$	
1	split : $w = T$	
2	$x \vee z$ $\bar{x} \vee \bar{y}$ $\bar{x} \vee y$ $x \vee y \vee \bar{z}$	
3	split : $x = T$	
4	\bar{y} y	
5	propagation : $y = F, y = T$ contradiction	
6	backtracking to stage 3 : $x = F$	
7	z $y \vee \bar{z}$	
8	propagation : $z = T, y = T$ solution : $w = T, x = F, y = T, z = T$	

Figure 1

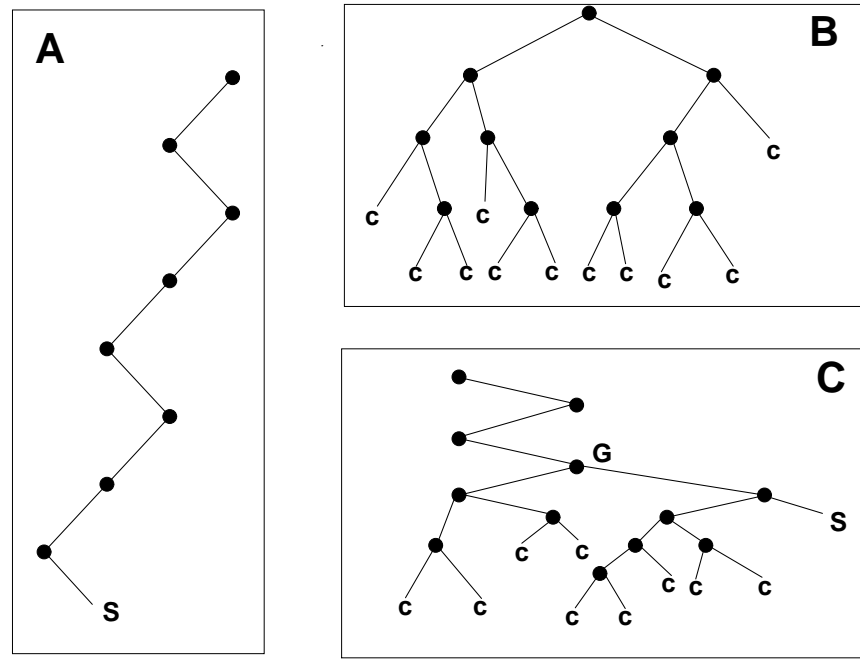


Figure 2

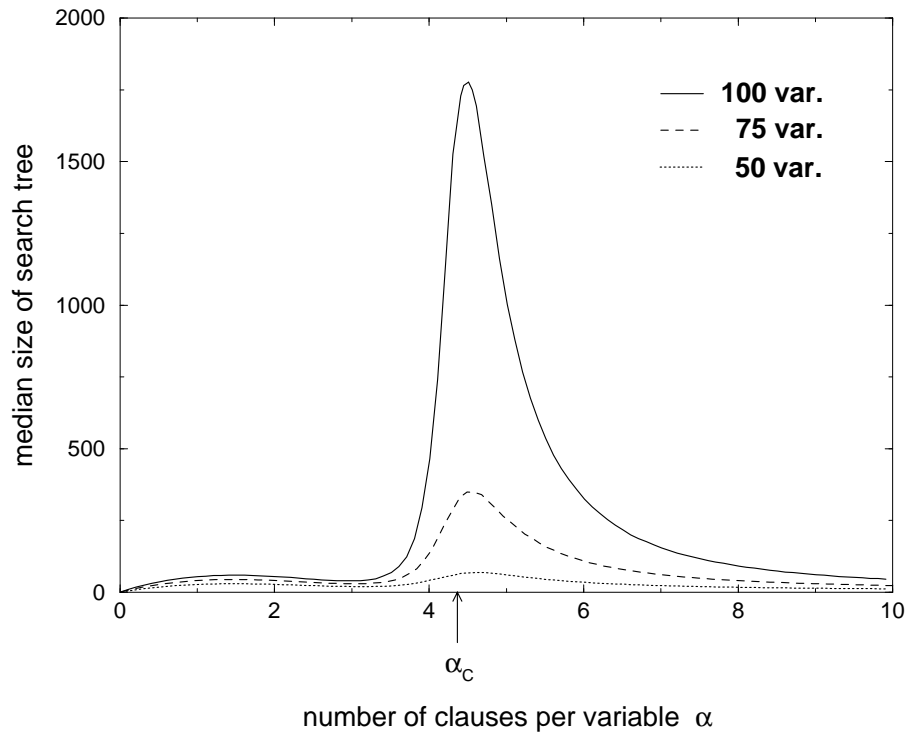


Figure 3

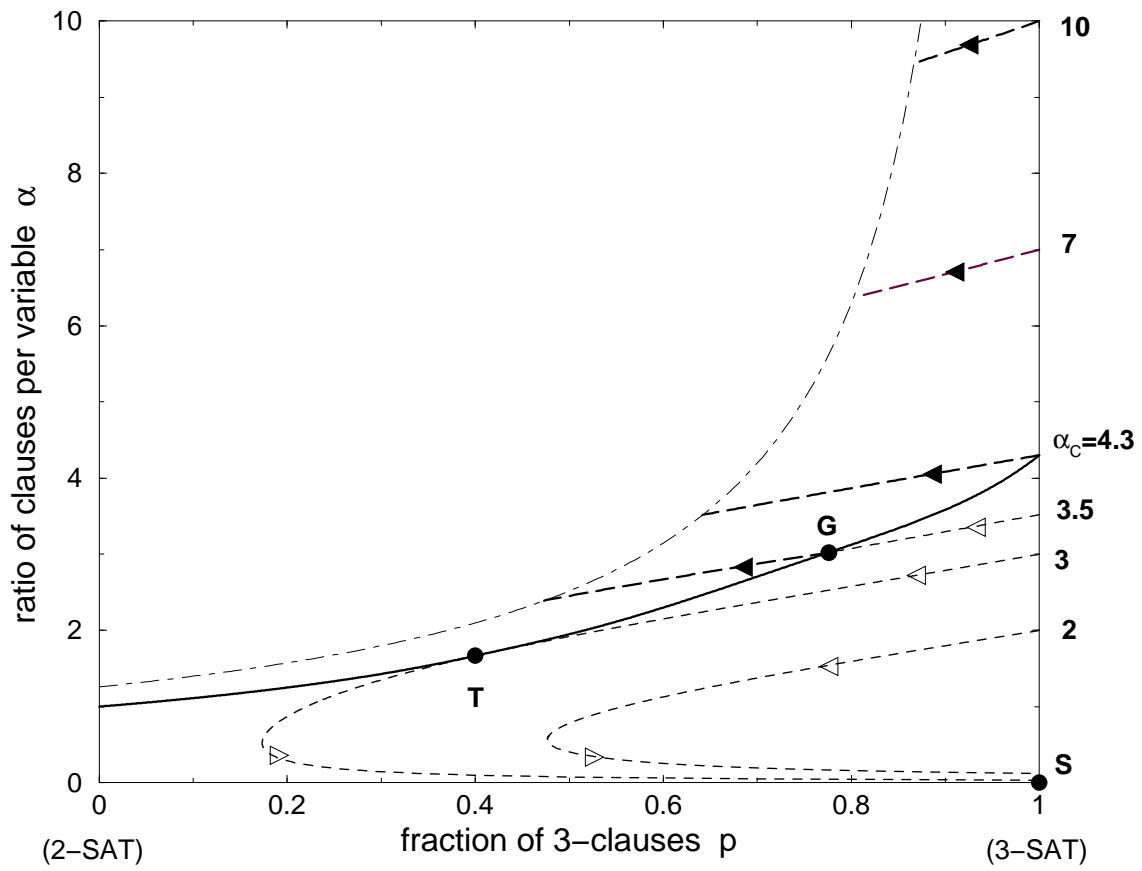


Figure 4